NUMERICAL INVESTIGATION OF SURFACE ROUGHNESS EFFECTS ON THE FLOW FIELD IN A SWIRL FLOW

Ali SAKİN [*]
İrfan KARAGÖZ [**]

Abstract: The aim of this study is to investigate axial and tangential velocity profiles, turbulent dissipation rate, turbulent kinetic energy and pressure losses under the influence of surface roughness for the swirling flow in a cyclone separator. The governing equations for this flow were solved by using Fluent CFD code. First, numerical analyses were run to verify numerical solution and domain with experimental results. Velocity profiles, turbulent parameters and pressure drops were calculated by increasing inlet velocity from 10 to 20 m/s and roughness height from 0 to 4 mm. Analyses of results showed that pressure losses are decreased and velocity field is considerably affected by increasing roughness height.

Keywords: Swirl flow, cyclone separators, roughness height

Bir Türbülanslı Akışta Akış Alan Üzerine Yüzey Pürüzlülüğü Etkisinin Sayısal İncelenmesi

Özet: Bu çalışmanın amacı, bir siklondaki girdaplı akışta yüzey pürüz yükseklik değerinin etkisinde eksenel ve teğetsel hız profilleri, türbülans yayınım oranı, türbülans enerjisi ve basınç kayıplarının araştırılmasıdır. Bu akış için korunum denklemleri Fluent CFD kodu kullanılarak çözülmüştür. İlk olarak sayısal model ve çözüm alanının doğrulanması için elde edilen veriler deneysel sonuçlarla karşılaştırılarak modelin doğrulaması yapılmıştır. Giriş hızı 10-20 m/s arasında ve pürüz yüksekliği 0 ile 4 mm arasında değiştirilerek, hız profilleri, türbülans parametreleri ve basınç kayıpları üzerindeki etkileri incelenmiştir. Analiz sonucunda pürüz yüksekliği arttıkça basınç kayıplarının azaldığı ve hız alanının önemli derecede etkilendiği görülmüştür.

Anahtar Kelimeler: Girdaplı akış, siklon ayırıcılar, pürüz yüksekliği

1. INTRODUCTION

Cyclone separators are widely used in industry for separating particles from a particulate flow. The typical geometrical layout of cyclone, used to separate particles from a fluid, depicted in Fig. 1a. The tangential velocity inlet generates the swirl dominated flow motion of fluid which forces particles toward the outer wall where they spiral in the downward direction. Eventually particles are collected in the dust bin (or flow through a dipleg) located at the bottom of the cyclone separator. The clean gas which is separated from the particles leaves through the exit pipe at the top. Swirl and turbulence are the two competing phenomena in the separation process; the swirl induces a centrifugal force on solid phase which is driving force behind the separation; turbulence disperses the solid particles and enhances the probability that particles get caught in

[*] TOFAS-FIAT Automotive Factory, Yeni Yalova Yolu Cad. No:574, Osmangazi, 16369 Bursa – TURKEY.
[**] Uludag University, Engineering Faculty, Dept. of Mechanical Engineering, Görükle, 16059 Bursa.
   Corresponding Author: A. Sakin (ali.sakin@tofas.com.tr)

the exit. Both phenomena are related to the particle size, and the flow conditions in the cyclone (Hoekstra et. al., 1999). Because of their simple structures, low maintenance and operational costs, they have high preference relative to other separation devices. Moreover, they have low pressure losses and relatively high particle collection efficiency. Karagoz and Avci (2005) calculated the pressure drop from the friction losses in cyclone body using a wall friction coefficient based on the surface roughness and the Reynolds number. They showed that the pressure drop coefficient increases considerably with Re at low Re values and remains almost constant at high Re values. Development of computer and numerical techniques, the use of computational fluid Dynamics (CFD) has received much attention in the simulation of cyclone flow and prediction of cyclone performance at different geometrical and operational parameters (Gong and Wang, 2004; Chuah et al., 2006; Karagoz and Kaya 2007, 2009; Kaya and Karagoz, 2008). Kaya and Karagoz (2012) studied the effects of exit pipe geometry on the pressure drop coefficient and the static pressure difference related to natural vortex length. They reported that pressure drop coefficient decreases with the increasing inlet velocity, becoming almost constant above a certain value of the inlet velocity due to effects of viscous forces decreases at high Reynolds numbers.

The aim of this study is to analyze the flow in a tangential inlet cyclone and investigate the effects of the surface roughness and the inlet velocity on the flow behavior and pressure losses.

2. MATHEMATICAL MODEL AND NUMERICAL PROCEDURE

2.1 Governing Equations

The air flow inside cyclone separator is generally time dependent and unstable. Therefore, flow was assumed to be three-dimensional, incompressible unsteady and turbulent in this study. Reynolds averaged Navier-Stokes (N-S) equations without body forces can be written as;

$$\frac{\partial \rho}{\partial t} + \frac{\partial (\rho U_i)}{\partial x_i} = 0 \tag{1}$$

$$\frac{\partial (U_i)}{\partial t} + U_j \frac{\partial U_i}{\partial x_j} = -\frac{1}{\rho}\frac{\partial P}{\partial x_i} + \frac{\partial}{\partial x_j}\left[v \frac{\partial U_i}{\partial X_j} - \overline{u_i' u_j'} \right] \tag{2}$$

for this flow. In Eq. (2) U_i is the time-average velocity, x_i is the position, P is the time-average pressure, ρ is the constant gas density, v is the kinematic viscosity and $\overline{u_i' u_j'}$ is the Reynolds stress tensor. Here, $u_i' = u_i - U_1$ is the ith fluctuating velocity component, where u_i is the instantaneous velocity.

The Reynolds stress tensor, $\overline{u_i' u_j'}$, represents co-relation between fluctuating velocities. It is an additional stress term due to turbulence and unknown factors and the RSM turbulence model was preferred to model this term (Karagoz and Kaya, 2009). Therefore, the transport equation for turbulence stress term can be written as;

$$\frac{\partial}{\partial t}(\overline{u_i' u_j'}) + \frac{\partial}{\partial x_k}(U_k \overline{u_i' u_j'}) = -\frac{\partial}{\partial x_k}\left(\overline{u_i' u_j' u_k'} + \frac{\overline{P' u_j'}}{\rho}\delta_{ik} + \frac{\overline{P' u_i'}}{\rho}\delta_{jk}\right)$$

Local time derivative C_{ij} = convection $D_{T,ij}$ = Turbulent diffusion

(3)

$$+\frac{\partial}{\partial x_k}\left[\nu\frac{\partial}{\partial x_k}(\overline{u_i' u_j'})\right] - \left(\overline{u_i' u_k'}\frac{\partial U_j}{\partial x_k} + \overline{u_j' u_k'}\frac{\partial U_i}{\partial x_k}\right) + \overline{\frac{p'}{\rho}\left(\frac{\partial u_i'}{\partial x_j} + \frac{\partial u_j'}{\partial x_i}\right)} - 2\nu\overline{\frac{\partial u_i'}{\partial x_k}\frac{\partial u_j'}{\partial x_k}}$$

$D_{L,ij}$= Molecular diffusion P_{ij}= Stress production φ_{ij}= Pressure strain ε_{ij}= Dissipation

Where P' is the fluctuating pressure and δ is the Kronecker delta. The terms C_{ij}, $D_{L,ij}$ and P_{ij} do not require modeling and can be solved explicitly, while $D_{T,ij}$, φ_{ij} and ε_{ij} need to be modeled to close the equations. However, the transport equations for these unknown factors could be derived from fundamental N-S equations, but this will create further closure problem.

In the fluent, the turbulent diffusion transport $D_{T,ij}$ is modeled in a simplified form of generalized gradient-diffusion hypothesis (Lien and Leschziner, 1994):

$$D_{T,ij} = \frac{\partial}{\partial x_k}\left[\frac{\mu_t}{\sigma_k}\frac{\partial \overline{u_i' u_j'}}{\partial x_k}\right]$$

(4)

Where $\sigma_k = 0.8$ and the turbulent viscosity μ_t is:

$$\mu_t = \rho C_\mu \frac{k^2}{\varepsilon}$$

(5)

where the constant $C_\mu = 0.08$, $k = \frac{1}{2}\overline{u_i' u_i'}$ is the turbulent kinetic energy and $\varepsilon = \frac{1}{2}\varepsilon_{ij}$ is the scalar dissipation rate.

The modeling of pressure strain term is most important, as it affects the redistribution of the Reynolds stresses and is expected to be significant for high swirl flow in cyclone separator, which features significant anisotropy. The pressure strain term is split into the following parts:

$$\phi_{ij} = \qquad \phi_{ij,1} \qquad + \qquad \phi_{ij,2} \qquad + \qquad \phi_{ij,w}$$

(6)

Slow pressure strain   Rapid pressure strain   Wall reflection term

$$\phi_{ij,1} = -C_1\frac{\varepsilon}{k}\left[\overline{u_i' u_j'} - \frac{2}{3}\delta_{ij}k\right]$$

(7)

$$\phi_{ij,2} = -C_2\left[(P_{ij} - C_{ij}) - \frac{2}{3}\delta_{ij}(P - C)\right]$$

(8)

Where P_{ij} and C_{ij} are defined as in Eq. (3); and $C_1 = 1.8, C_2 = 0.6$ are constants $P = \frac{1}{2}P_{kk}$, and $C = \frac{1}{2}C_{kk}$.

$$\phi_{ij,w} = C_1' \frac{\varepsilon}{k}\left(\overline{u_k'u_m'}n_k n_m \delta_{ij} - \frac{3}{2}\overline{u_i'u_k'}n_j n_k - \frac{3}{2}\overline{u_j'u_k'}n_i n_k\right)\frac{C_\mu^{\frac{3}{4}}k^{\frac{3}{2}}}{K\varepsilon d} \tag{9}$$

In Eq.(9) n_k is the x_k component of the unit normal to the wall, d is the normal distance to the wall, K is the von Karman constant (=0.4187); and $C_1' = 0.50, C_2' = 0.30$ and $C_\mu = 0.09$ are constants. The turbulent kinetic energy k is modeled by taking the trace of the Reynolds stress tensor.

However, if the value of k is required at boundaries, the fluent solves addition transport equation of k as:

$$\frac{\partial}{\partial t}(\rho k) + \frac{\partial}{\partial x_j}(\rho k U_j) = \frac{\partial}{\partial x_j}\left[\left(\mu + \frac{\mu_t}{\sigma_k}\right)\frac{\partial k}{\partial x_j}\right] + \frac{1}{2}P_{ij} - \rho\varepsilon \tag{10}$$

The dissipation tensor ε_{ij} is assumed isotropic and is approximated as:

$$\varepsilon_{ij} = \frac{2}{3}\delta_{ij}\rho\varepsilon \tag{11}$$

The scalar dissipation rate ε can be computed form a model transport equation:

$$\frac{\partial}{\partial t}(\rho\varepsilon) + \frac{\partial}{\partial x_j}(\rho\varepsilon U_j) = \frac{\partial}{\partial x_j}\left[\left(\mu + \frac{\mu_t}{\sigma_\varepsilon}\right)\frac{\partial\varepsilon}{\partial x_j}\right] + \frac{1}{2}C_{\varepsilon 1}P_{ij}\frac{\varepsilon}{k} - C_{\varepsilon 2}\rho\frac{\varepsilon^2}{k} \tag{12}$$

where $\sigma_k = 0.82, \ \sigma_\varepsilon = 1.0, \ C_{\varepsilon 1} = 1.44$ and $C_{\varepsilon 2} = 1.92$ are constants.

2.2 Law-of-the-Wall Modified for Roughness

Experiments in roughened pipes and channels indicate that the mean velocity distribution near rough walls, when plotted in the usual semi-logarithmic scale, has the same slope $(1/\kappa)$ but a different intercept (additive constant B in the log-law). Thus, the law-of-the-wall for mean velocity modified for roughness has the form:

$$\frac{u_p u^*}{\tau_w/\rho} = \frac{1}{\kappa}\ln\left(E\frac{\rho u^* y_p}{\mu}\right) - \Delta B \tag{13}$$

where $u^* = C_\mu^{1/4}k^{1/2}$ and ΔB is a roughness function that quantifies the shift of the intercept due to roughness effects (Cebeci and Bradshaw, 1977).

ΔB depends, in general, on the type (uniform sand, rivets, threads, ribs, mesh-wire, etc.) and size of the roughness. There is no universal roughness function valid for all types of roughness. For a sand-grain roughness and similar types of uniform roughness elements, however, ΔB has been found to be well-correlated with the nondimensional roughness height, $K_s^+ = \rho K_s u^*/\mu$, where K_s is the physical roughness height and $u^* = C_\mu^{1/4}k^{1/2}$. Analyses of experimental data show that the roughness function, ΔB, is not a single function of K_s^+, but

takes different forms depending on the K_s^+ value. It has been observed that there are three distinct regimes (Cebeci and Bradshaw, 1977):

- Hydrodynamically smooth ($K_s^+ < 3{\sim}5$)
- Transitional ($3{\sim}5 < K_s^+ < 70{\sim}90$)
- Fully rough ($K_s^+ > 70{\sim}90$)

According to the data, roughness effects are negligible in the hydrodynamically smooth regime, but become increasingly important in the transitional regime, and take full effect in the fully rough regime.

In Fluent, the whole roughness regime is subdivided into the three regimes, and the formulas proposed by Cebeci and Bradshaw based on Nikuradse's data (Cebeci and Bradshaw, 1977) are adopted to compute the roughness function, ΔB, for each regime.

For the hydrodynamically smooth regime ($K_s^+ < 2.25$):

$$\Delta B = 0 \tag{14}$$

For the transitional regime ($2.25 < K_s^+ < 90$):

$$\Delta B = \frac{1}{\kappa} \ln\left[\frac{K_s^+ - 2.25}{87.75} + C_{K_s} K_s^+ \right] \times \sin\{0.4258(\ln K_s^+ - 0.811)\} \tag{15}$$

where C_{K_s} is a roughness constant, and depends on the type of the roughness.

In the fully rough regime ($K_s^+ > 90$):

$$\Delta B = \frac{1}{\kappa} \ln\left[1 + C_{K_s} K_s^+ \right] \tag{16}$$

In the solver, given the roughness parameters, the roughness function $\Delta B(K_s^+)$ is evaluated using the corresponding formula (Eq.14, Eq.15 or Eq.16). The modified law-of-the-wall in Eq.13 is then used to evaluate the shear stress at the wall and other wall functions for turbulent quantities.

2.3 Setting the Roughness Parameters

To model the wall roughness effects, two roughness parameters: the Roughness Height (K_s), and the Roughness Constant (C_{K_s}) are defined. The default roughness height (K_s) is zero, which corresponds to smooth walls. For the roughness to take effect, a non-zero value for K_s is specified. For a uniform sand-grain roughness, the height of the sand-grain can simply be taken for K_s. For a non-uniform sand-grain, however, the mean diameter (D_{50}) would be a more meaningful roughness height. For other types of roughness, an equivalent sand-grain roughness height should be used for K_s. Choosing a proper roughness constant (C_{K_s}) is dictated mainly by the type of the given roughness. The default roughness constant ($C_{K_s} = 0.5$) was determined so that, when used with $k - \epsilon$ turbulence models, it reproduces Nikuradse's resistance data for pipes roughened with tightly-packed, uniform sand-grain roughness. Some experimental evidence shows that, for non-uniform sand-grains, ribs, and wire-mesh roughness, a higher value ($C_{K_s} = 0.5{\sim}1.0$) is more appropriate. Unfortunately, a clear guideline or directions for choosing C_{K_s} for arbitrary types of roughness is not available.

To have a mesh size such that wall-adjacent cell is smaller than the roughness height is not physically meaningful for best results the distance from the wall to centroid of the wall adjacent cell must be greater than K_s. For this study standard wall function was selected as near wall treatment so it is not necessary to create fine mesh close to the cyclone wall. Roughness constant was taken as default value ($C_{K_s} = 0.5$) during all computations.

2.4 Computational Mesh

The cyclone model with tangential inlet used in this study is given in Fig.1a. Flow volume was divided into a number of computational cells by using Icem CFD software, as can be seen in Fig.1b and 1c.

(a)   **(b)**   **(c)**
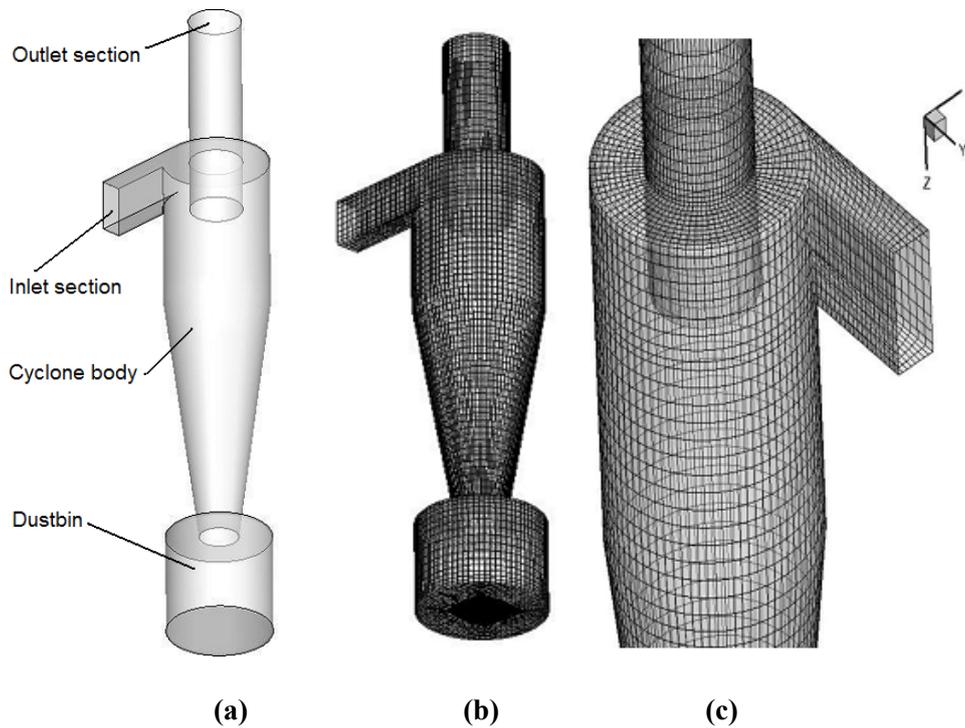
Figure 1:
The geometry of the cyclone and computational mesh used in the numerical solutions

Since the standard wall function was used in the turbulence model, very fine mesh was not required near the cyclone walls. However, fine mesh structure was used in the core region where strong gradients in the flow parameters were present. In order to verify the numerical solution, the cyclone geometry and experimental data reported by Hoekstra (2000) were used in this study. The diameter (D) of the cyclone used in this study is 290 mm. The dimensions and the planes where experimental measurements were taken are given in Fig. 2 and Table 1. A number of tests have been performed to achieve grid independent solutions. It has been observed that 127000 cells provide sufficient grid independency and results are in good agreement with experimental data as explained in 2.7 Validation Section. Wall y+ values are around 200 for this mesh.
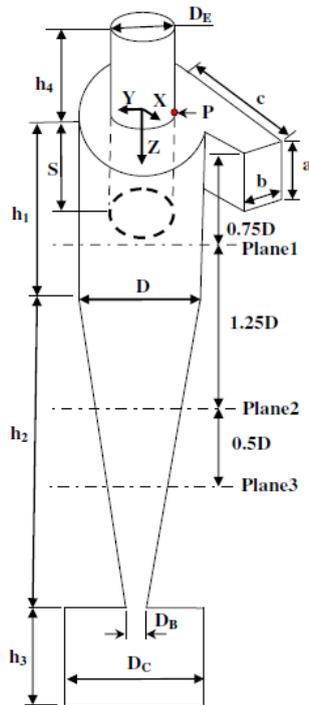
Table 1. Cyclone dimensions

Dimension	Size
a	0.5D
b	0.2D
c	0.85D
D_B	0.37D
D_c	1.0D
D_E	0.5D
h_1	1.5D
h_2	2.5D
h_3	1.0D
h_4	1.5D
S	0.5D

Figure 2:
Details of cyclone geometry and plane
locations used for numerical investigation
(Shukla et. al. 2010)

2.5 Boundary Conditions

Air was assumed to enter the cyclone with uniform velocity. No slip boundary conditions were used at the cyclone walls and outflow boundary condition was applied at the exit. Table 2 summarizes the boundary conditions

Table 2. Boundary conditions

Air density (kg/m^3)	1.225
Viscosity of air (kg/ms)	1.7894E-5
Inlet velocity (U_{in}) (m/s)	16.1
Turbulence intensity (I)	0.1 (%10)
Hydraulic diameter (m)	0.082857
Exit: Outflow – flow rate	1
Walls	No slip condition

To analyze roughness effect in computational domain, wall boundary condition roughness height was taken as 0 (smooth), 0.15, 0.5, 1, 2 and 4 mm. Computational results obtained with inlet velocity of 16.1 m/s are used for comparison with experimental data given in the literature.

2.6 Solution Algorithm

Based on the study of Kaya and Karagoz (2008), governing equations of three-dimensional, incompressible flow inside the cyclone Eq. (1, 2) and the RSM turbulence equations were discretized over the computational cells and iteratively solved by using Fluent software. Since it

is relatively straight forward and has been successfully implemented in numerous CFD procedures, SIMPLEC algorithm was used for pressure velocity coupling in this study. PRESTO (Pressure Staggering Option) scheme was chosen for the pressure interpolation as it was shown to be well suited for steep pressure gradients involved in complex swirling flows. Second order upwind differencing discretization scheme was chosen for momentum, and first order upwind scheme was used for turbulence stresses. Unsteady, second order implicit scheme was chosen for all computations and 0.0001 s was taken as time step.

2.7 Validation

The quality of a numerical solution can be verified by the comparison of the results to the experimental results. Experimental results for the same cyclone were taken from the works reported by Shukla et. al. (2010). Comparison between the computational and experimental velocity profiles are given in Fig. 3 for inlet velocity of 16.1 m/s in dimensionless form.
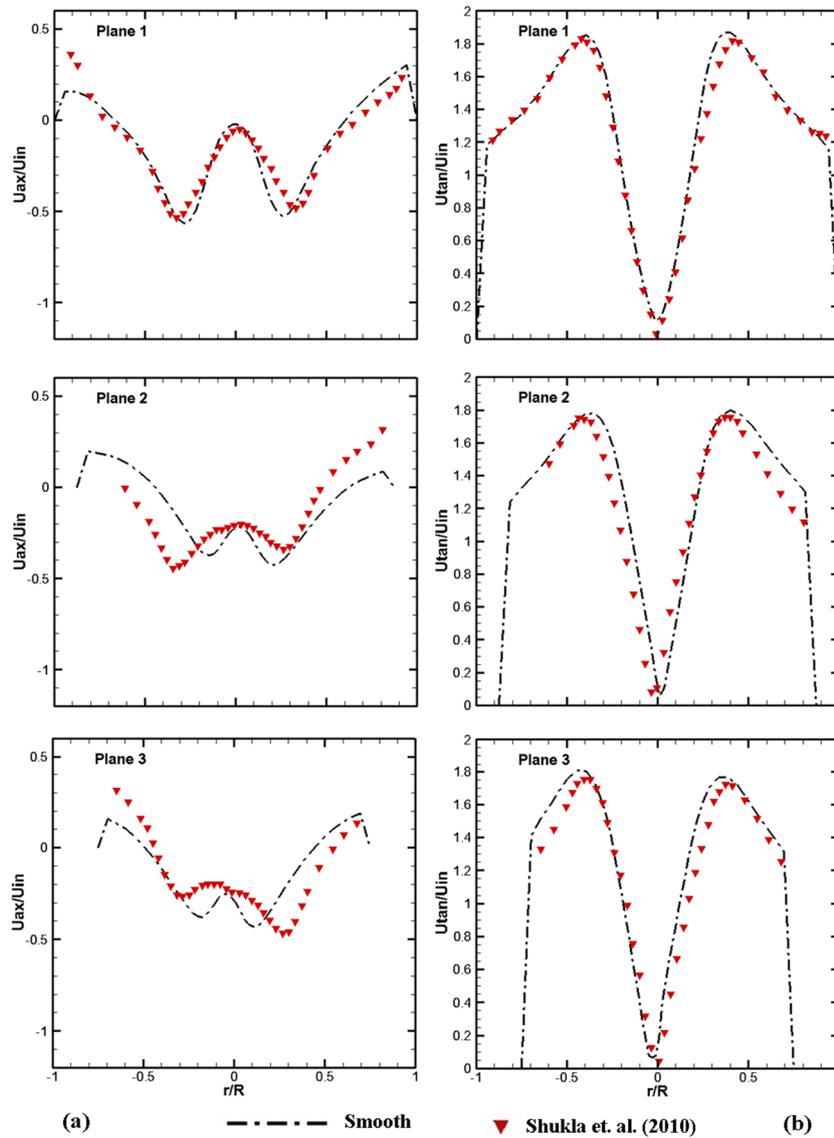
Figure 3:
Dimensionless tangential and axial velocity profiles at three planes along the cyclone (U_{in}= 16.1 m/s)

8

As can be seen from the Fig. 3b, very good agreement was obtained for tangential velocity profiles at all planes. The axial velocity profiles do not agree well with the experimental values except for the plane 1 (Fig. 3a). However, variation in the axial velocity profiles shows similar behavior qualitatively with the experimental findings.

Static pressure contours are given in Fig. 4b at the mid-plane of the cyclone. The inner vortex where low pressure prevails can be seen clearly in the core region. The vortex attain at the bottom of the dustbin. Static pressure computed by Shukla et. al. (2010) at the top wall of the cyclone also show very good agreement with the present calculations (Fig. 4a). Pressure drop over the cyclone was calculated as 1057 Pa for the inlet velocity of 16.1 m/s.

(a)   **(b)**
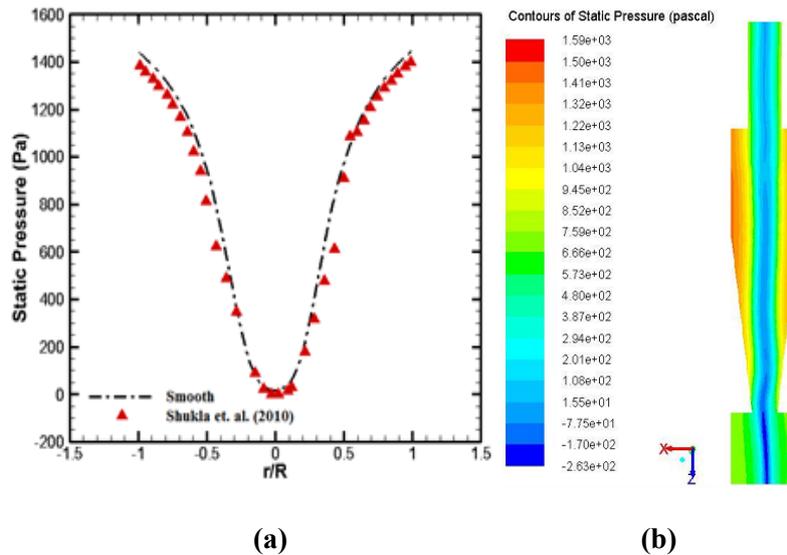
Figure 4:
*Static pressure distributions at the top (a) and at the mid-plane (b) of the cyclone*

3. RESULTS AND DISCUSSION

Fig. 5 represents the comparison of dimensionless tangential and axial velocity profiles with experimental values for different surface roughness at plane 1, plane 2 and plane 3. The numerical solutions for smooth and small roughness give both mean tangential (Fig. 5b) and axial velocity profiles (Fig. 5a) close to measured values in the entire domain of cyclone separator. The experimental data mostly lie between the smooth and small roughness cases. Tangential velocity profiles of 2 and 4 mm have different profiles in accordance with other profiles. Axial velocity profiles are in good agreement, tangential velocity profiles for roughness height 2 and 4 mm show different behavior from the other profiles.
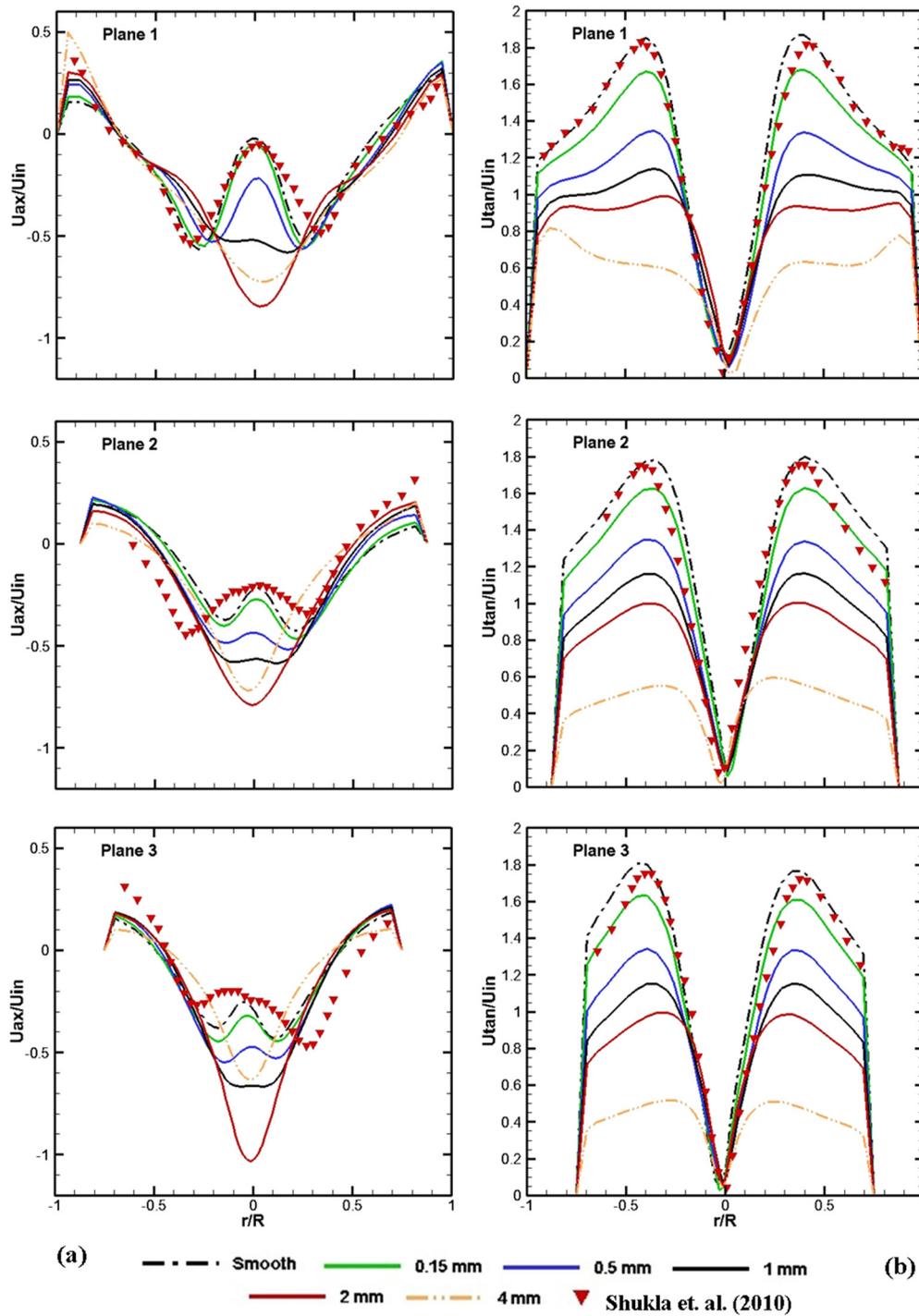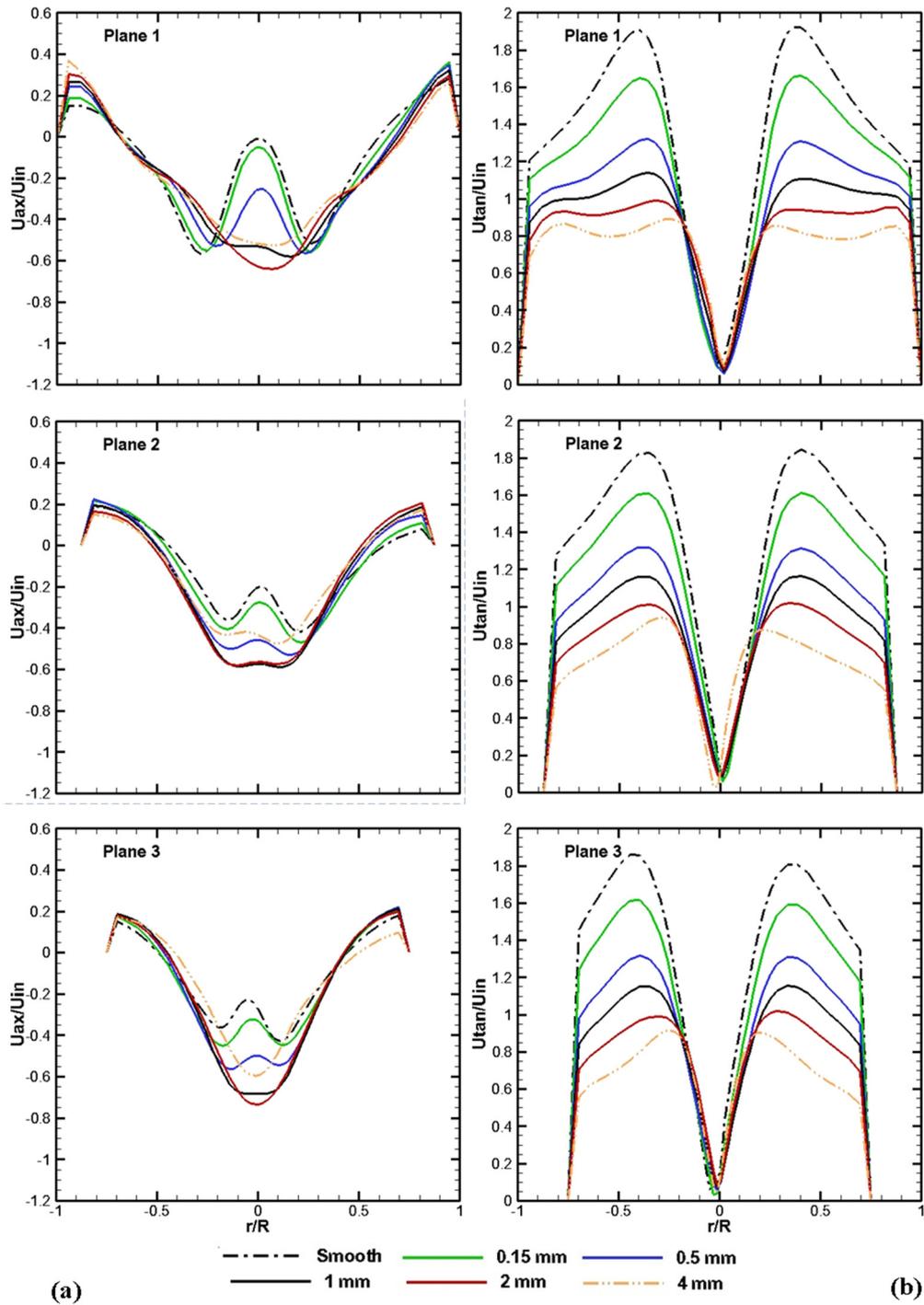
Figure 5:
Tangential and axial velocity profiles for U$_{in}$= 16.1 m/s

Fig. 6 represents the comparison of dimensionless tangential and axial velocity profiles for U$_{in}$= 10 m/s under the influence of different roughness heights. As is the case with U$_{in}$= 16.1 m/s, results both for axial and tangential velocity profiles are similar for all section planes. Velocity profiles behavior for 2 and 4 mm roughness height is the same as previous profile.
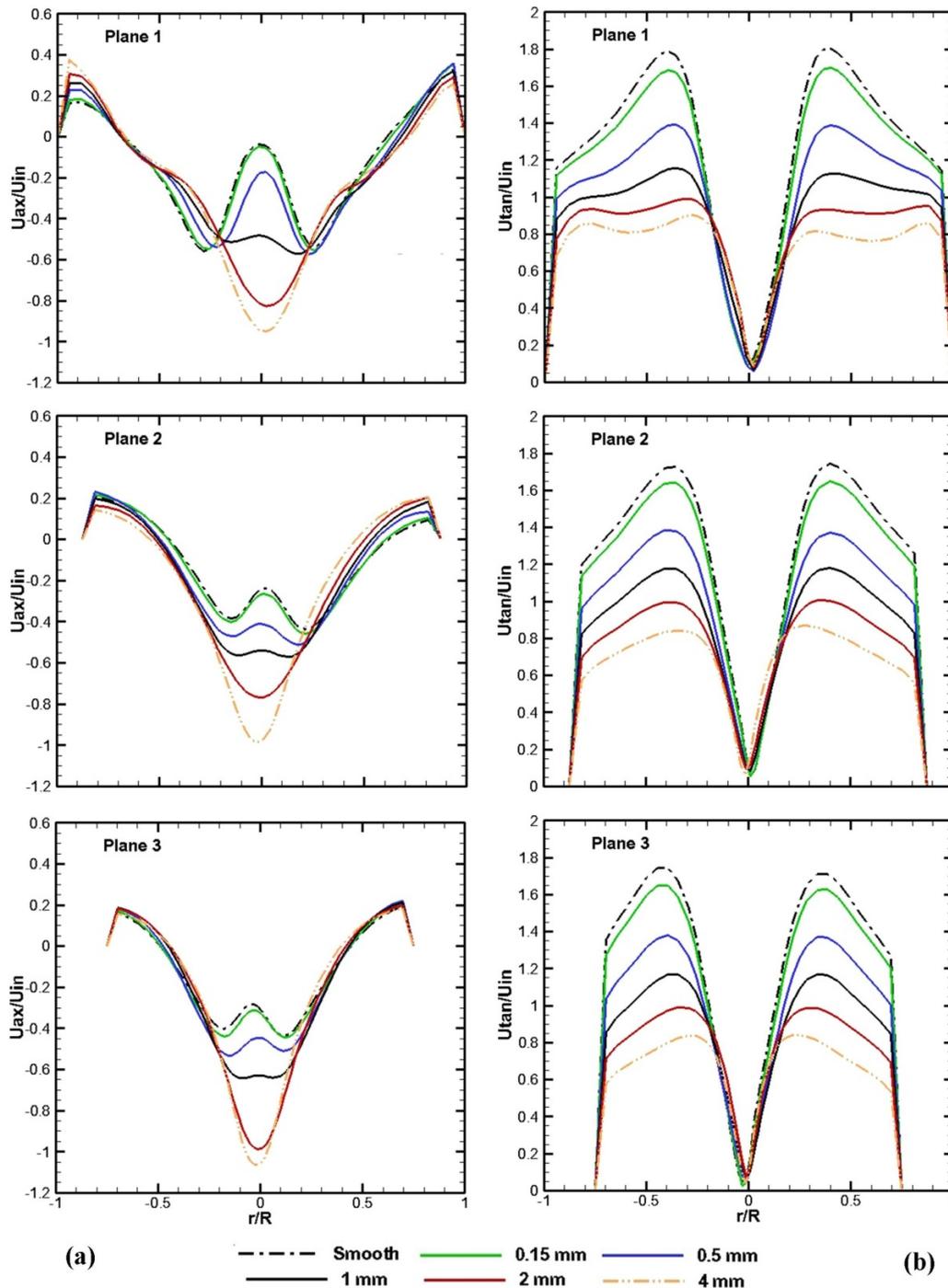
Figure 6:
Tangential and axial velocity profiles for U_{in}= 10 m/s

Influence of roughness heights on the dimensionless tangential and axial velocity profiles for U_{in}= 25 m/s is given comparatively in Fig. 7. Results for both axial and tangential velocity profiles are similar for all section planes. Velocity profiles behavior for 2 and 4 mm roughness height is the same as previous.
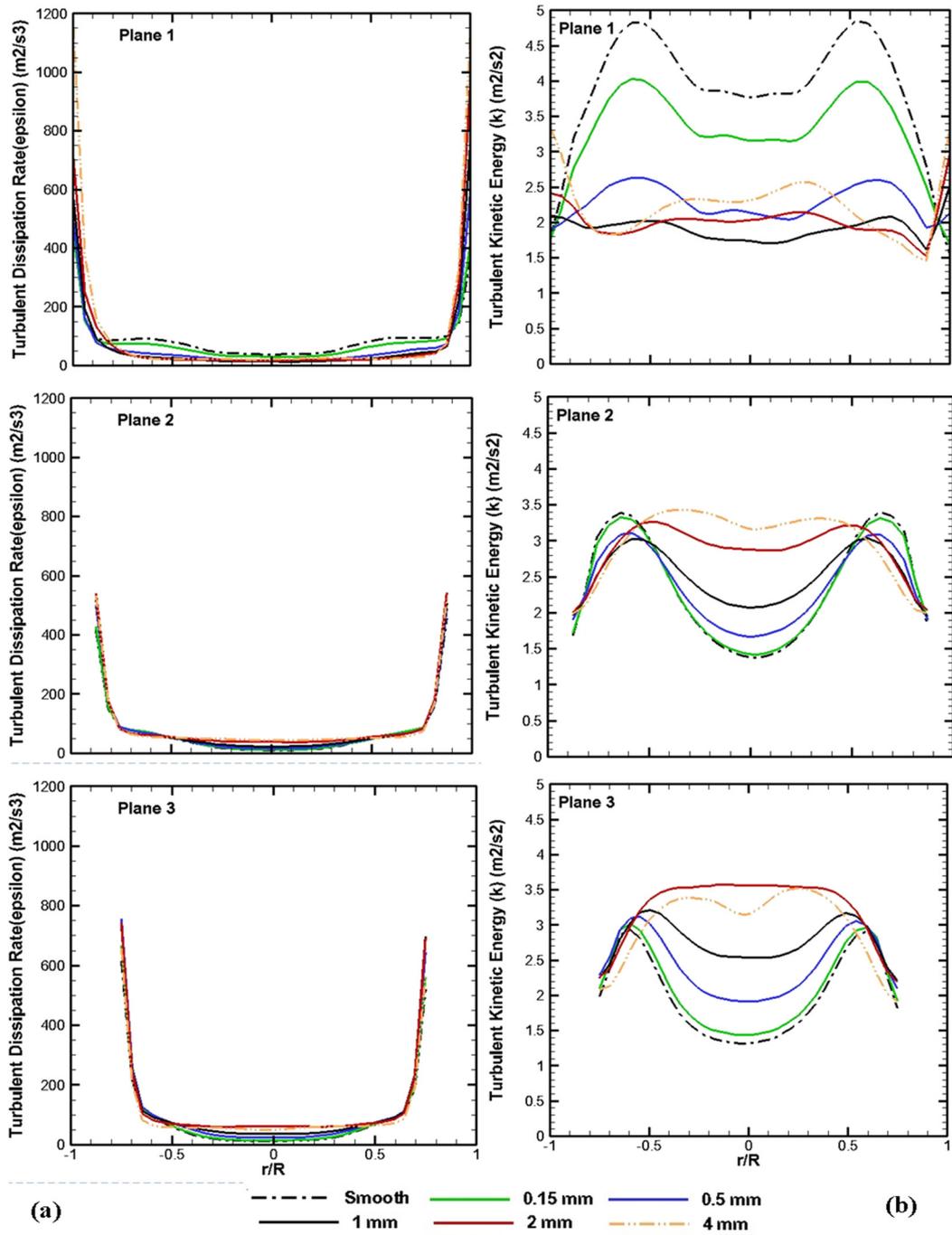
Figure 7:
*Tangential and axial velocity profiles for $U_{in}= 25$ m/s*

As can be seen that, tangential velocity profiles for all inlet velocities are similar and maximum roughness height (4 mm) gives the minimum velocity profile for all cases.

Increase of inlet velocity increases friction losses as expected but the role of surface roughness height needs to be explained. As it is seen from the results, increase of surface roughness height

decreases pressure loss. Because when the surface roughness height increases, swirl cannot be accelerated enough to follow trajectory and a part of flow involves to inner vortex as short circuit before reaching end of the conical section. This situation also can be seen from axial velocity profiles. Thus increase of roughness height reduces tangential velocity and so pressure loss decreases. Although decrease of pressure loss is seen as positive it is a disadvantage in terms of particle separation efficiency. Because decrease of inlet velocity worsens particle separation efficiency and this is not a desired situation.

Figure 8:
Turbulent dissipation rate and turbulent kinetic energy for U$_{in}$=10 m/s
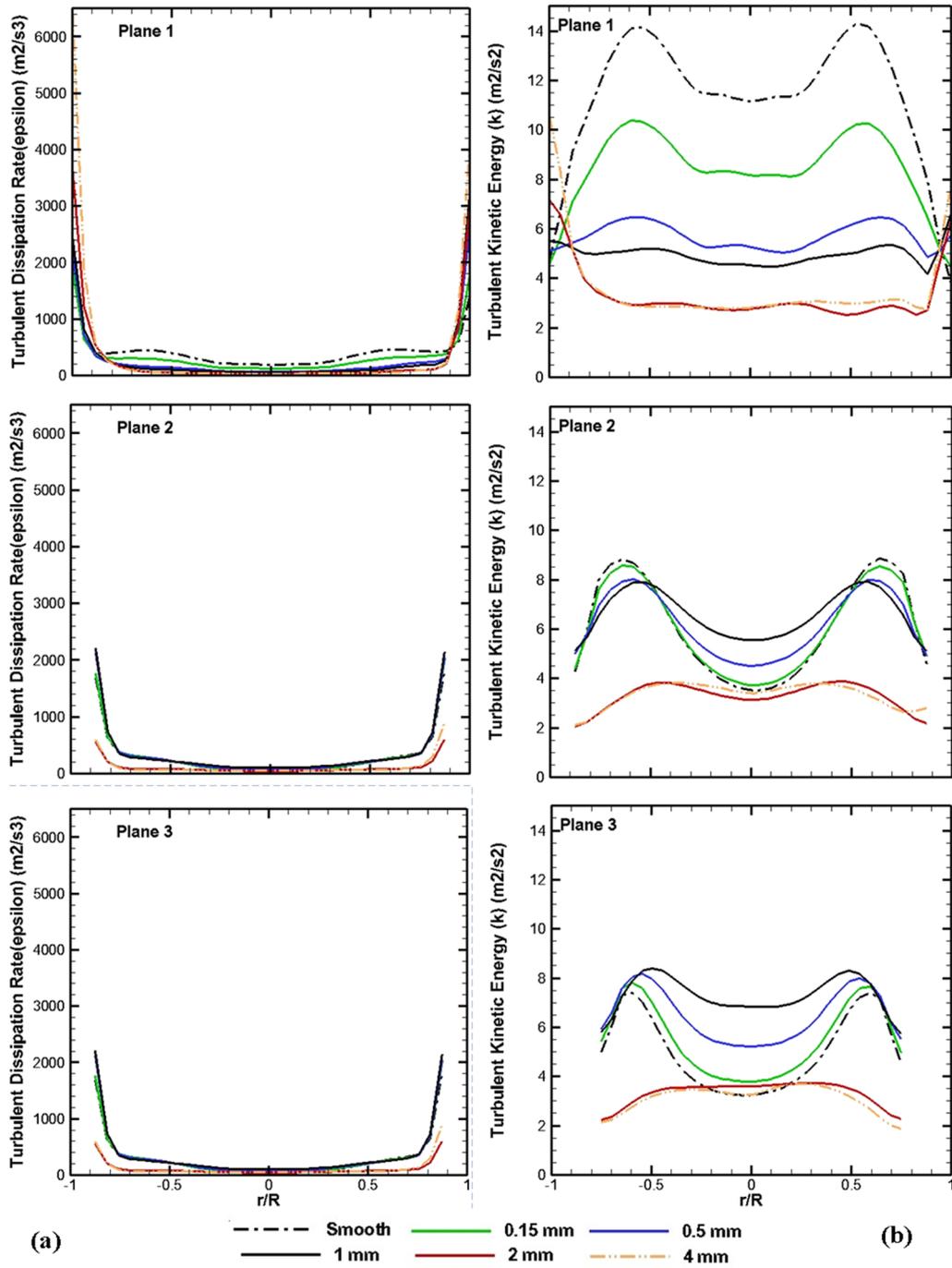
Figure 9:
Turbulent dissipation rate and turbulent kinetic energy for U_{in}=16.1 m/s
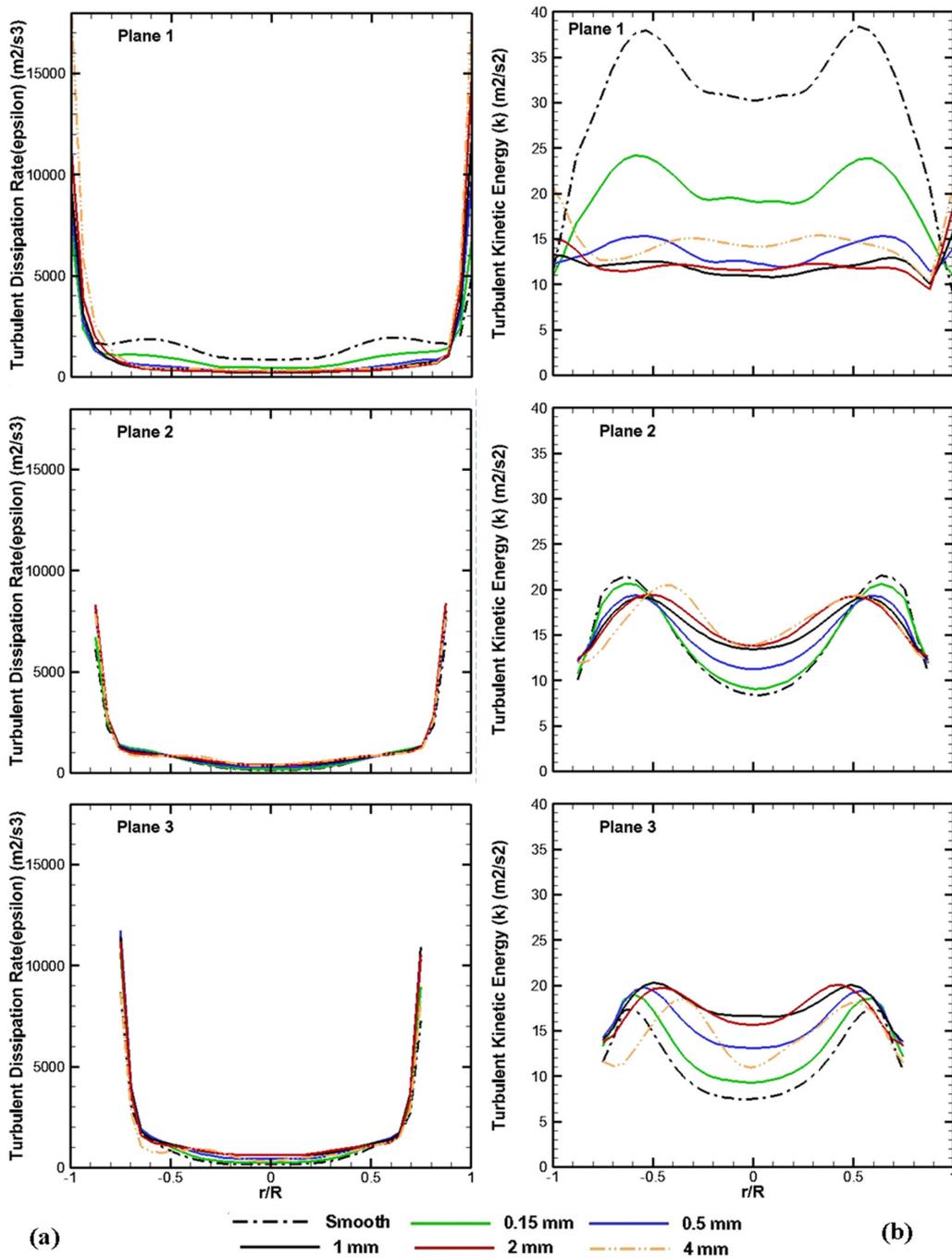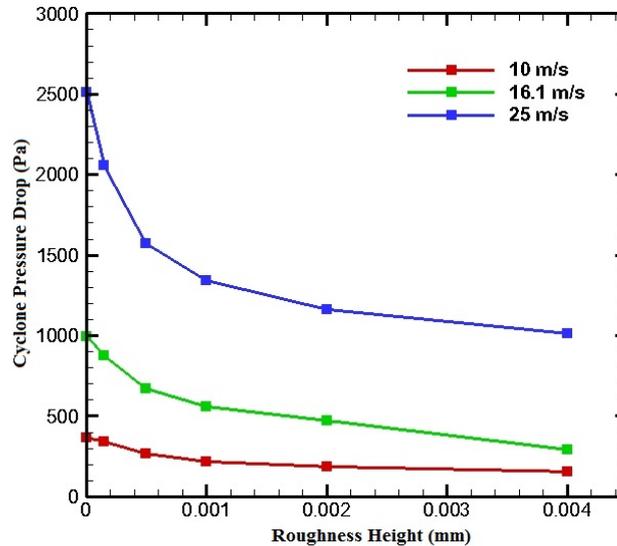
Figure 10:
Turbulent dissipation rate and turbulent kinetic energy for U_{in}=25 m/s

Turbulent dissipation rate and turbulent kinetic energy distributions under the influence of roughness height for input velocities 10 and 16.1 m/s are given in Fig. 8 and 9. Similar profiles were obtained for the velocity of 25 m/s (Fig. 10). Turbulent dissipation rate profiles are close to each other and dissipation rate is increasing by input velocity. Turbulent kinetic energy profiles for plane 1, has the same behavior for all input velocities.

All these results showed that roughness height plays an important role, especially on tangential velocity and turbulent kinetic energy distributions. Separation of particles in a cyclone

takes places under the influence of centrifugal forces which are directly related to tangential velocity. Since tangential velocity decreased considerably with increasing surface roughness, it is possible to say that an increase in surface roughness will lead to a decrease in particle collection efficiency.

Figure 11:
Pressure losses influence of roughness height for U_{in}=10, 16.1 and 25 m/s

Net static pressure losses have been computed between inlet and outlet. Influence of roughness height on the pressure losses is given in Fig. 11. As it is seen in Fig. 11, pressure losses is decreasing by greater roughness height and also increasing with greater input velocities. Therefore, maximum pressure loss occurs at 25 m/s input velocity and smooth wall conditions.

4. CONCLUSIONS

A tangential inlet reversed flow cyclone which has a very complex swirling flow was considered in this study. Mathematical modeling and numerical solution of the flow was presented. The numerical results obtained by the RSM turbulence model together with the standard wall function were compared with the experimental results given in the literature. Very good agreement was obtained for tangential velocity profiles and static pressure distributions.

Axial and tangential velocity profiles were computed for different inlet velocities and similar distribution form obtained under the influence of roughness height. The maximum tangential velocity decreased considerably with increasing surface roughness for all cases. Maximum dissipation rate and kinetic energy distribution have obtained by increasing input velocity.

It is concluded from the results that the increase of gas inlet velocity increases the separation efficiency, but it also increases the pressure drop. The tangential velocity in the cyclone is reduced by increasing wall roughness, due to increase in flow resistance and decay of swirl. Also Increase of roughness height reduces tangential velocity and so pressure loss decreases. Although decrease of pressure loss is seen as positive it is a disadvantage in terms of particle separation efficiency. Because decrease of inlet velocity worsens particle separation efficiency and this is not a desired situation.

Results show that surface roughness considerably affected velocity and turbulent kinetic energy distributions in a cyclone. Therefore, surface roughness should also play an important role on the cyclone performance.

ACKNOWLEDGEMENTS

REFERENCES

1. Cebeci, T. and Bradshaw P. (1997) *Momentum Transfer in Boundary Layers*, Hemisphere Publishing Corporation, New York.

2. Chuah, T. G., Gimbun, J. and Choong, T. S. Y. (2006) A CFD Study the Effect of Cone Dimensions on Sampling Aerocyclones Performance and Hydrodynamics, *Powder Technology*, 162, 126–132.

3. Gong, A. L. and Wang, L. Z. (2004) Numerical Study of Gas Phase Flow in Cyclones with the Repds. *Aerosol Science and Technology*, 38, 506–512.

4. Hoekstra, A. J., Derksen, J. J. and Van Der Akker, H. E. A. (1999) An Experimental and Numerical Study of Turbulent Swirling Flow in Gas Cyclone, *Chemical Engineering Science,* 54, 2055-2065.

5. Hoekstra, A. J. (2000) Gas Flow Field and Collection Efficiency of Cyclone Separators, Ph.D. Thesis, Delft University of Technology, Netherlands.

6. Karagoz, I. and Avci, A. (2005) Modelling of the Pressure Drop in Tangential Inlet Cyclone Separators, *Aerosol Science and Technology*, 39, 857–865.

7. Karagoz, I. and Kaya, F. (2007) CFD Investigation of the Flow and Heat Transfer Characteristics in A Tangential Inlet Cyclone*, International Communications in Heat and Mass Transfer*, 34, 1119–1126.

8. Karagoz, I. and Kaya, F. (2009) Evaluations of Turbulence Models for Highly Swirling Flows in Cyclones*, Computer Modeling in Engineering and Sciences,*43(2),111-129.

9. Kaya, F. and Karagoz, I. (2008) Performance Analysis of Numerical Schemes in Swirling Turbulent Flows in Cyclones, *Current Science*, 94, 1273–1278.

10. Kaya, F. and Karagoz, I. (2012) Experimental and Numerical Investigation of Pressure Drop Coefficient and Static Pressure Difference in a Tangential Inlet Cyclone Separator, *Chemical Papers*, 66(11), 1019–1025.

11. Lien, F. S. and Leschziner, M. A. (1994) Assessment of Turbulence-Transport Models Including Non-Linear RNG Eddy-Viscosity Formulation and Second –Moment Closure for Flow over A Backward Facing Step, *Computers & Fluids,* 23, 983-1004.

12. Shukla, S. K., Shukla, P. and Ghosh, P. (2010) Evaluation of Numerical Schemes Using Different Simulation Methods for the Continuous Phase Modeling of Cyclone Separators, *Advanced Powder Technology*, DOI:10.1016/j.apt.2010.11.009.